IOP Publishing Journal of Micromechanics and Microengineering
J. Micromech. Microeng. **31** (2021) 044001 (11pp) https://doi.org/10.1088/1361-6439/abec1c

Integrated 3D printed microfluidic circuitry and soft microrobotic actuators via *in situ* direct laser writing

Abdullah T Alsharhan[1], Olivia M Young[1], Xin Xu[2], Anthony J Stair[1] and Ryan D Sochol[1,2,3,4,*]

[1] Department of Mechanical Engineering, University of Maryland, College Park, MD 20742, United States of America
[2] Fischell Department of Bioengineering, University of Maryland, College Park, MD 20742, United States of America
[3] Robert E. Fischell Institute of Biomedical Devices, University of Maryland, College Park, MD 20742, United States of America
[4] Maryland Robotics Center, University of Maryland, College Park, MD 20742, United States of America

E-mail: rsochol@umd.edu

Received 1 December 2020, revised 5 February 2021
Accepted for publication 4 March 2021
Published 19 March 2021

Abstract

Over the past two decades, researchers have advanced and employed integrated microfluidic circuitry to enable a wide range of chemical and biological 'lab-on-a-chip' capabilities. Yet in recent years, a wholly different field, soft robotics, has begun harnessing microfluidic circuitry as a promising means to enhance soft robot autonomy. Unfortunately, key challenges associated with not only the fabrication of microfluidic circuitry, but also its integration with soft robotic systems represent critical barriers to progress. To overcome such issues, here we present a strategy that leverages '*in situ* direct laser writing (*is*DLW)'—a submicron-scale additive manufacturing (or 'three-dimensional (3D) printing') approach developed previously by our group—to fabricate microfluidic circuit elements and soft microrobotic actuators directly inside of enclosed microchannels. In addition, we introduce 'normally closed' microfluidic transistors that comprise free-floating sealing discs designed to block source-to-drain fluid flow until the application of a target gate pressure. As an exemplar, we printed microfluidic transistors with distinct gate activation properties as well as identical soft microgrippers downstream of each drain within 40 μm-tall microchannels. Experimental results for a source pressure of 100 kPa revealed that microgripper deformation was prevented in the absence of a gate input; however, increasing the gate pressure to 300 kPa induced actuation of one set of microgrippers, while a further increase to 400 kPa led to both sets of microgrippers actuating successfully. These results suggest that the presented *is*DLW-based strategy for manufacturing and integrating 3D microfluidic circuit elements and microrobotic end effectors could offer unique potential for emerging soft robotic applications.

* Author to whom any correspondence should be addressed.

Supplementary material for this article is available online

Keywords: additive manufacturing, 3D printing, direct laser writing, two-photon polymerization, microfluidic circuitry, soft robotics, microrobotics

(Some figures may appear in colour only in the online journal)

1. Introduction

Historically, the manufacturing of miniaturized fluidic systems has relied predominantly on micromachining methods developed for the semiconductor and microelectromechanical systems industries [1]. Motivated by the benefits inherent to manipulating fluids at smaller scales (e.g. for chemistry and biology) [2, 3], researchers initially focused on adapting such microfabrication protocols for microfluidic device construction [4]. Consequently, the earliest microfluidic systems comprised standard, mechanically stiff semiconductor industry materials, such as silicon [5] and glass [6, 7], until the introduction of 'soft lithography' [8]. Building upon the elastomeric replication methods of Bell Labs [9], the Whitesides group reported a technique for molding and bonding silicone elastomers to form enclosed microchannels [10]. The Quake group harnessed an extension of this protocol in which multiple, discrete layers of micromolded elastomeric materials (and/or membranes) are bonded together—termed 'multilayer soft lithography'—to demonstrate a novel microfluidic valve capable of actively regulating fluid flow via a control input [11]. This capability gave rise to the first generation of integrated fluidic circuits (IFCs), which investigators employed for a diversity of chemical, biological, and biomedical applications [12–14].

In response to the increasing numbers of microfluidic valves incorporated into IFCs, and in turn, the demands for off-chip equipment required to perform on-chip fluidic processes—i.e. the so-called 'tyranny of microfluidic interconnects'—investigators have explored additional strategies to realize IFCs with autonomous functionalities [15]. Drawing inspiration from electronic circuitry, researchers pioneered a second generation of IFCs by adapting multilayer soft lithography to achieve fundamental fluidic analogues, including two-layer fluidic capacitors [16], three-layer fluidic diodes [16, 17] and 'normally open' fluidic transistors [17], and five-layer (normally open) pressure-gain fluidic transistors [18]. Although IFCs based on such components found only limited use in chemical and biological communities over the past decade, the emergence of 'soft robotics'—classes of robots based on compliant materials that are actuated via fluidic means—has reinvigorated interest in self-regulating IFCs [19–21]. In particular, Wehner *et al* leveraged their previously reported multi-layer soft lithography-based microfluidic oscillator [17] to successfully demonstrate an untethered soft 'octobot' capable of autonomous, periodic actuation of its tentacles [22]. Unfortunately, multi-layer soft lithography protocols suffer from a wide range of drawbacks, including: (i) time- and labor-intensive manufacturing processes, (ii) limited device reproducibility (e.g. due to manual alignment and bonding procedures), (iii) access and training-based restrictions associated with microfabrication clean rooms and equipment, and (iv) geometric (e.g. '2.5D') limitations inherent to photolithography and micromolding [23–25]. Consequently, there is significant interest in alternative methodologies for IFC construction [26, 27].

Recently, a third generation of IFCs has emerged founded on the use of additive manufacturing (or colloquially, 'three-dimensional (3D) printing') technologies [28]. Although our group and others have demonstrated the ability to fabricate microfluidic circuitry using a variety of additive manufacturing approaches, including extrusion-based printing (e.g. direct ink writing) [29], vat photopolymerization (e.g. stereolithography) [30–34], and material jetting (e.g. multijet modeling and PolyJet printing) [35–37], such efforts have remained at relatively large scales (e.g. in the submillimeter-to-millimeter rather than sub-100 μm range) and only involved 'normally open' microfluidic transistor operational modes [29–31, 35]. To leverage the unparalleled precision and geometric versatility of 'direct laser writing (DLW)' [38, 39] for microfluidic circuit element manufacturing, our group recently introduced an approach termed '*in situ* direct laser writing (*is*DLW)' by which 3D microfluidic components can be printed directly inside of—and notably, fully sealed to—enclosed microchannels [40, 41]. We demonstrated that 3D microfluidic spring diodes [40] and (normally open) microfluidic bellow-type transistors [41] could be printed with feature resolutions on the order of 100 nm. In this work, we build on our recent developments in *is*DLW-based microfluidic circuitry to explore 'normally closed' 3D microfluidic transistor architectures that allow for gate activation characteristics to be customized geometrically. With respect to soft robotics [42–44], and in particular, soft microrobotics applications that rely on soft actuators [45–47], such as soft microgripper-based medical catheters [48], we investigate an *is*DLW-printed microfluidic system comprising soft microgrippers integrated with distinct microfluidic transistors for which all microgripper actuation states are regulated by the magnitude of a single gate pressure input.

2. Materials and methods

2.1. (isDLW)-based 'normally closed' microfluidic transistor and soft microgripper concepts

An important trade-off associated with the high resolution afforded by DLW is that the size of the cured volume element or 'voxel'—i.e. located at the point of two-photon (or multi-photon) polymerization—is ill suited for printing the macro-to-micro interfaces (e.g. fluidic access ports) required

for microfluidic applications [49–51]. To circumvent this issue, we previously reported an *is*DLW strategy by which critical 3D microfluidic components (i.e. those that necessitate the geometric versatility of DLW) could be printed within a bulk, enclosed (2.5D) microfluidic system, while supporting full fluidic sealing between the microchannel walls and the printed components [40, 41]. Although we demonstrated this concept for microchannel materials including polydimethylsiloxane (PDMS) [40] and the thermoplastic, cyclic olefin polymer (COP) [41], experimental results revealed COP to be a far superior substrate for direct attachment of DLW-printed components to the microchannel compared to PDMS [40, 41, 52]. Thus, here we employ COP–COP microdevices for the bulk microfluidic system in which the microfluidic circuit elements and soft microrobotic grippers are printed.

The fabrication of the normally closed microfluidic transistors and soft microgrippers involves two primary stages: (i) DLW-enabled construction of the bulk COP–COP microfluidic device (figure 1(a)), and (ii) *is*DLW of the microfluidic transistors and soft microgrippers within the bulk system (figures 1(b)–(d)). The *is*DLW approach in this work entails infusing a liquid-phase photocurable material into the enclosed COP–COP microfluidic device (figure 1(a)), and then selectively polymerizing the material in a point-by-point, layer-by-layer manner to print the soft microgrippers (figure 1(b)) and microfluidic transistors (figure 1(c)) directly inside of (and fully sealed to) the channels. Following completion of the printing process, residual (i.e. uncured) photomaterial is evacuated from the device and the print is developed (figure 1(d)).

The operation of the soft microgrippers is similar to that of established soft actuators at larger scales [53, 54]. In the absence of a fluidic input, both actuators remain in their undeformed states (figure 1(e)). Upon the application of a fluidic input of sufficient magnitude, however, the two mirrored actuators comprising asymmetric bellows inflate in a manner that yields deformation toward one another (figure 1(f)). In soft robotics communities, such components are typically modeled as fluidic capacitors [22]. To facilitate the normally closed operational functionality of the 3D microfluidic transistor, the component is initially printed with a free-floating sealing disc (i.e. without support structures) positioned above an orifice and a bellow microstructure that comprises a central micropost on the top surface (figure 1(g)). Under an applied source pressure (P_S), microfluidic forces induce sealing of the disc atop the orifice, thereby obstructing the flow of fluid through the component (figure 1(h)). By applying a gate pressure (P_G) of sufficient magnitude, however, the bellows expand such that the micropost physically disengages the disc from the orifice to promote source-to-drain fluid flow (Q_{SD}) (figure 1(i)). As with prior works, one caveat to the electronic analogy is that, although fluidic transistors are gate-regulated three-terminal components, they exhibit operating characteristics akin to electronic transistors biased in the triode region [35].

2.2. COP–COP microdevice fabrication

The fabrication methods are based on our previously reported COP-based *is*DLW protocols [41]. The negative master mold of the microchannels was designed using the computer-aided design (CAD) software, SolidWorks (Dassault Systemes, France). Because straight microchannel sidewalls disrupt fluidic sealing for *is*DLW-printed components [40, 41], the microchannel mold consists of trapezoidal channels with heights of 40 μm and widths of 60 μm with 30° tapered sidewalls. The CAD models were exported in the STL file format, and then imported into the computer-aided manufacturing (CAM) software, DeScribe (Nanoscribe GmbH, Germany), to generate the laser writing path code. Si substrates (25 mm × 25 mm) were prepared via successive rinses with acetone and isopropyl alcohol (IPA), and then dried with inert N_2 gas before being placed on a 100 °C hot plate for 15 min. A drop of the negative-tone photoresist, IP-S (Nanoscribe), was dispensed onto the center of the prepared Si substrate, which was then loaded into the Nanoscribe Photonic Professional GT printer (laser wavelength = 780 nm). The molds were printed using the 25× objective lens in the 'dip-in laser lithography (DiLL)' mode configuration with a laser power of 30 mW. Following the DLW-printing process, the substrate was developed via successive rinses with propylene glycol monomethyl ether acetate (PGMEA) for 30 min and IPA for 2 min to eliminate any residual photomaterial.

To microreplicate the microchannel mold using COP, a 3 mm-thick sheet of COP (ZEONOR 1060 R, Zeon Corp., Japan) was rinsed with IPA, dried with N_2 gas, and then hot embossed at 120 °C for 3 min. Through holes for the fluidic access ports were drilled in the molded COP at desired inlet and outlet locations. To enclose the microchannels, a 100 μm-thick COP film (microfluidic ChipShop GmbH, Germany) was exposed to vapor-phase cyclohexane at 30 °C for 2 min, after which the film and the micropatterned COP sheet were immediately brought into contact for 1 min at room temperature (20 °C–25 °C) to yield COP–COP bonding.

2.3. isDLW-based printing of microfluidic transistors and soft microgrippers

All of the 3D microfluidic transistor and soft microgripper components were designed using SolidWorks (Dassault Systemes) and exported in the STL file format. The STL files were imported into DeScribe (Nanoscribe) CAM software to generate the laser writing path code. The negative-tone photoresist, IP-L 780 (Nanoscribe), was loaded into the enclosed microchannels of the COP–COP device. The microdevice was then loaded into the Nanoscribe Photonic Professional GT printer with immersion oil placed on the underside of the COP film. Each 3D microfluidic component was printed ('ceiling-to-floor') in a serial fashion using the 63× objective lens in the oil-immersion mode configuration with laser powers ranging from 16 to 30 mW [41] and scan speeds of 10–20 mm s^{-1}. Following the DLW printing process, residual photomaterial was evacuated from the

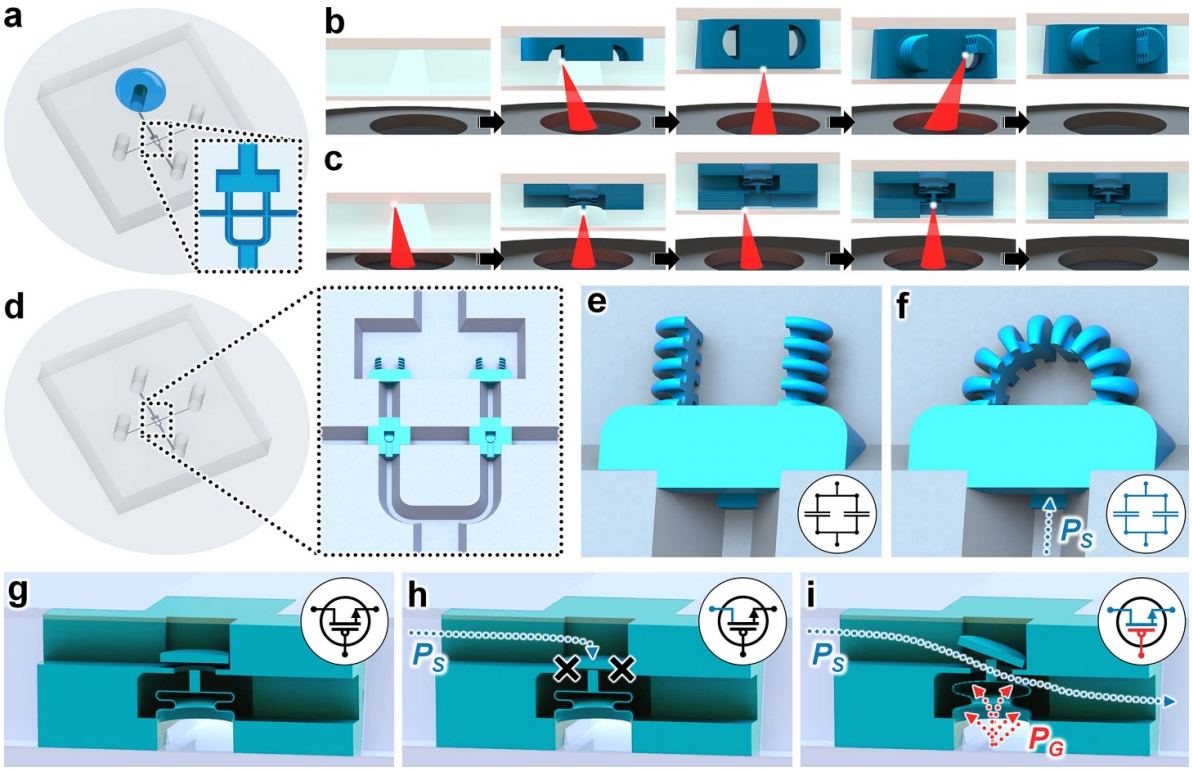

Figure 1. Conceptual illustrations of the '*in situ* direct laser writing (*is*DLW)' strategy for 3D printing 'normally closed' microfluidic transistors and soft microgrippers in a cyclic olefin polymer (COP) microfluidic system. (a) Infusion of a liquid-phase photomaterial into an enclosed COP–COP microdevice. (b), (c) A focused femtosecond IR laser selectively polymerizes the photomaterial to print the: (b) soft microgrippers, and (c) 'normally closed' microfluidic transistors (rotated cross-sectional view). (d) Printed microfluidic components (comprising cured photomaterial) that are fully adhered to the luminal surface of the COP–COP microchannel at designed locations. (e), (f) Soft microgripper operating principle. (e) 'Open State'. In the absence of an input, the microgrippers remain undeformed and apart. (f) 'Closed State'. An applied source pressure (P_S) input causes the asymmetric bellows to inflate, which results in the actuators deforming toward one another. (g)–(i) 'Normally closed' microfluidic transistor operating principle (rotated cross-sectional view). (g) Initial state directly after printing. (h) 'Closed State'. In the absence of a gate input, an applied P_S input causes the free-floating disc to seal atop the central orifice, thereby obstructing source-to-drain fluid flow (Q_{SD}). (i) 'Open State'. Under the application of a gate pressure (P_G) of sufficient magnitude, the bellow microstructure expands in a manner that causes the central micropost to physically displace the sealing disc from the orifice to promote Q_{SD}.

microdevice through successive infusions of PGMEA for 10 min, IPA for 3 min, and pressurized air.

2.4. Optical characterization

Scanning electron microscopy (SEM) characterizations were performed using a TM4000 tabletop SEM (Hitachi, Tokyo, Japan). The low-vacuum environment of the SEM allowed for the systems and components to be imaged without the need for conductive coatings. To support SEM imaging of the microfluidic transistor and microgripper, microstructures were printed in unenclosed microchannels (i.e. without the 100 μm-thick COP film). In addition, the design of the microfluidic transistor was modified to facilitate a partially open, cross-sectional view, which included a support structure to hold the disc in its initial position.

2.5. Theoretical simulations

Finite element analysis (FEA) simulations of microfluidic transistors were conducted using the commercial software, COMSOL Multiphysics v.5.3a (COMSOL, Inc. Sweden). The FEA simulations were performed using the fluid–structure interaction (FSI) module under stokes flow conditions and quasi-static structural transient behavior. The solid elements were modeled as the photomaterial, IP-L 780 ($E = 1.75$ GPa and $\nu = 0.49$) [55], while the input fluid was modeled as water ($\rho = 10^3$ kg m^{-3}; $\eta = 8.9 \times 10^{-4}$ Pa s). The pressure applied at the gate region was assigned to the interior surface of the bellow microstructure and was modeled as a boundary load to simulate the operating conditions. To simplify the computation, the sealing disc was set to be fixed atop the micropost. The simulations were performed for a constant P_S of 10 kPa, with P_G increasing from 0 to 100 kPa by increments of 10 kPa.

2.6. Microfluidic experimentation

All of the microfluidic experiments were conducted using the Fluigent microfluidic control system and flow rate platform coupled with MAESFLO software (Fluigent, France). Fluids were infused into the COP device using fluorinated ethylene propylene tubing (Cole-Parmer, Vernon Hills, IL)

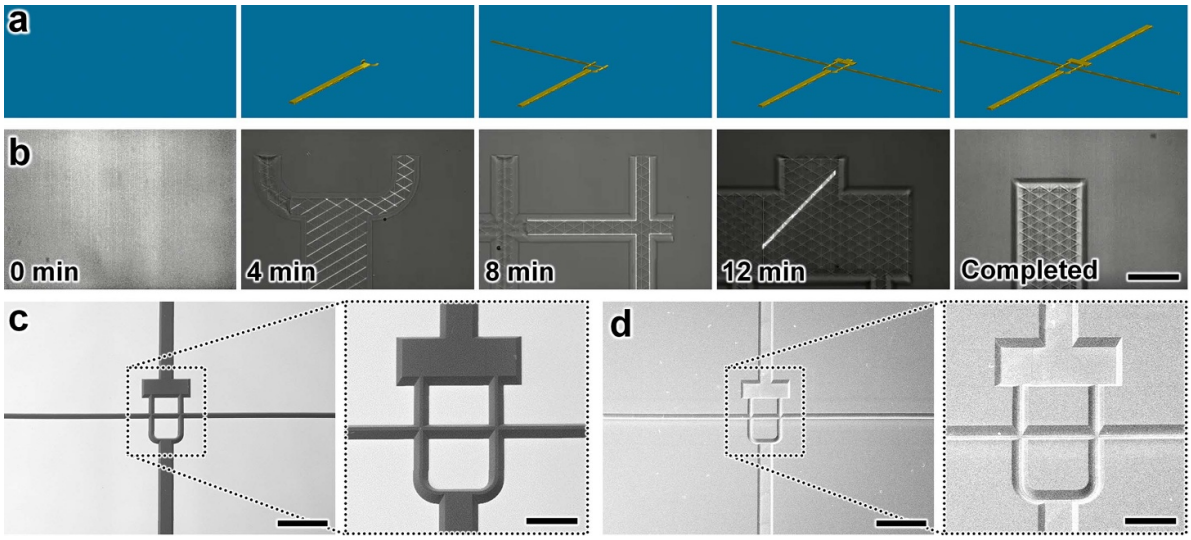

Figure 2. Fabrication results for DLW-printing of the trapezoidal microchannel negative master mold and subsequent COP-based microreplication. (a), (b) Sequential (a) computer-aided manufacturing (CAM) simulations, and (b) corresponding micrographs of the DLW printing process (see Movie 1). Total time ≈ 16 min; Scale bar = 50 μm. (c), (d) SEM micrographs of the (c) DLW-printed master mold, and (d) hot embossing-replicated COP sheet. Scale bars = 500 μm; Expanded view scale bars = 100 μm.

and stainless-steel catheter couplers (20 ga., Instech, Plymouth Meeting, PA). For testing with fluorescently labeled fluids, rhodamine B and methylene blue dyes (MilliporeSigma, St. Louis, MO) were infused into the microdevices via source and gate inlet ports, respectively. Brightfield microscopy was performed using an inverted microscope (Motic AE31, Motic, Canada) connected to a charge-coupled device (CCD) camera (Moticam Pro 285B, Motic), while fluorescence imaging was performed using an inverted fluorescence microscope (Axio Observer.Z1, Zeiss, Germany) connected to a CCD camera (Axiocam 503 Mono, Zeiss). Experiments were performed by setting the magnitude of the P_S input to three distinct, constant pressures: 50, 100, and 150 kPa. The gate output was sealed using stainless steel catheter plugs (Instech), while the P_G input was increased from 0 to 400 kPa at a rate of 1 kPa s^{-1} corresponding to each P_S magnitude (with three trials performed for each P_S). Data from the experiments were collected and processed using MATLAB software (MathWorks, Natick, MA) to quantify Q_{SD} with respect to the varying P_S and P_G conditions. Experimental results are presented in the text as mean ± standard deviation (S.D.).

3. Results and discussion

3.1. isDLW-based integrated microfluidic system fabrication

CAM simulations and corresponding micrographs of fabrication results for DLW-based printing of the negative master mold are shown in figures 2(a) and (b), respectively. Due to the large print area of the channel mold structures (approximately 5 mm × 5 mm), we employed a stitching-based print methodology by which the master mold was printed in 300 μm × 300 μm areas that connect together. This process resulted in a total print time of approximately 16 min (figure 2(b); Movie 1). The print time could be reduced dramatically by using an objective lens with a lower magnification (e.g. 10×). One caveat to using a lower magnification objective lens is that the feature resolution would be diminished slightly; however, it is unlikely such a change would negatively affect the mold as it consists of simple (2.5D) geometries. SEM micrographs revealed effective printing of the 40 μm-tall, 30°-tapered trapezoidal microchannel molds (figure 2(c)) and its microreplication using the COP sheet (figure 2(d)).

The *is*DLW strategy for additively manufacturing the 'normally closed' microfluidic transistors involved two primary steps: (i) printing the outer structure-microchannel interfacing components as well as the bellow microstructure (wall thickness designed to be 500 nm) and central micropost (diameter = 4 μm), and then (ii) printing the free-floating sealing disc (thickness = 2 μm) within the rectangular compartment (figures 3(a) and (b); Movie 2). The quasi-static flow conditions within the system allowed for the sealing disc to be printed without any support structures. The total print time for the 40 μm-tall microfluidic transistor was approximately 9 min (figure 3(b); Movie 2). For *is*DLW of the microgrippers, the fabrication process consisted of three steps: (i) printing of the structure-microchannel interfacing component, (ii) printing one soft actuator, and then (iii) printing the remaining soft actuator (figures 3(c) and (d); Movie 3). The total print time for a complete soft microgripper (i.e. consisting of two soft actuators) was less than 6 min (figure 3(d); Movie 3). SEM micrographs of fabrication results for a microfluidic transistor and a soft microgripper are presented in figures 3(e) and (f), respectively.

3.2. 'Normally closed' microfluidic bellow-type transistors

We performed FEA FSI simulations under a constant P_S and varying P_G to provide insight into the operational behavior of an ideal 'normally closed' 3D microfluidic transistor

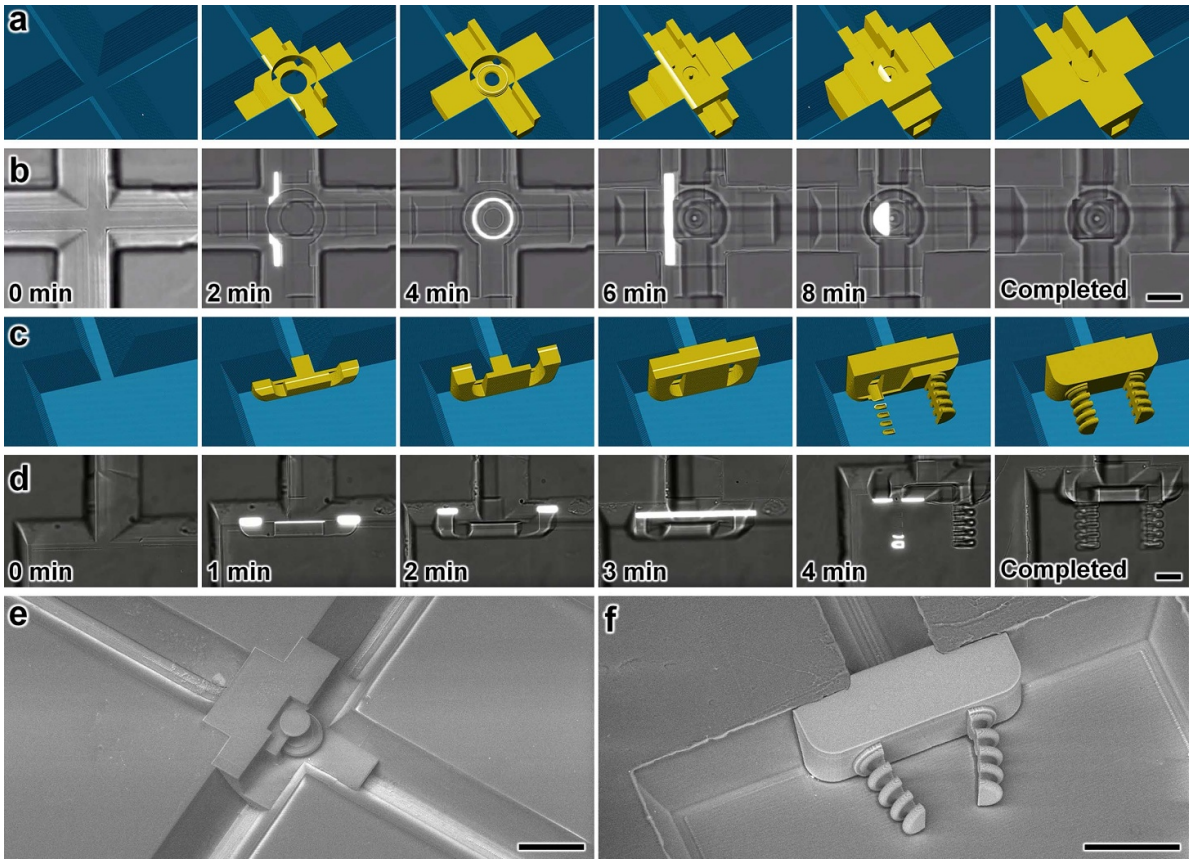

Figure 3. Fabrication results for *is*DLW-printing of 'normally closed' microfluidic transistors and soft microgrippers. (a)–(d) Sequential (a), (c) CAM simulations, and (b), (d) corresponding micrographs of the *is*DLW printing process for a: (a), (b) 'normally closed' microfluidic transistor (total time ≈ 9 min; see Movie 2), and (c), (d) soft microgripper (total time ≈ 6 min; see Movie 3). Scale bars = 25 μm. (e), (f) SEM micrographs of a: (e) 'normally closed' microfluidic transistor cross section, and (f) soft microgripper. Scale bars = 50 μm.

(figures 4(a) and (b)). In the absence of a P_G input, Q_{SD} remained fully blocked; however, increasing the magnitude of P_G caused the bellow microstructure to expand, thereby displacing the disc away from the orifice and facilitating Q_{SD} (figure 4(a)). The simulation results revealed a key constraint for the presented design as cases associated with P_G inputs that are too high could cause the bellow microstructure to inflate to such a degree that its top surface physically seals along the underside of the orifice—similar to sealing behavior of the 'normally open' 3D microfluidic transistor reported previously [41]. Such phenomena provide a basis for the decreasing slopes of the Q_{SD}-P_G relationships exhibited at higher P_G (figure 4(b)). One caveat to the simulation results is that, by setting the sealing disc as a moving boundary (i.e. the disc's position is determined by the micropost's location), the fluidic forces onto the disc were not considered. Although this simplification could lead to variations between theoretical and experimental results, we expect that divergences from the disc's planar orientation (as modeled) to an inclined configuration (e.g. figure 1(i)) would likely enhance the P_G-mediated 'open state' Q_{SD} performance.

We conducted preliminary optical characterizations of the *is*DLW-printed microfluidic transistor by infusing fluids into the device and then using both brightfield (figure 4(c)) and fluorescence (figure 4(d)) microscopy to evaluate performance. For example, applying a P_S without a P_G input caused the disc to instantly moved toward the central orifice; however, applying a P_G input resulted in optically observable displacements of the sealing disc away from the orifice (figure 4(c); Movie 4). In addition, we investigated the capacity for the microfluidic transistor to isolate the source-to-drain and gate flow paths—a critical requirement for operational functionality—by loading two distinct fluorescently labeled fluids corresponding to each flow path (figure 4(d)). The fluorescence microscopy results revealed that the two distinct fluorescence signatures were successfully maintained within their respective channels, without any visible signs of undesired cross-contamination found in either opposing flow path (figure 4(d)).

A fundamental benefit inherent to additive manufacturing technologies is the ability to readily customize the geometries of printed components. For the microfluidic transistor, a number of geometric factors could be adjusted to alter its performance [41, 56], such as the dimensions of the bellow microstructure (e.g. wall thickness, number of bellows, bellow diameter) as well as the diameter of the sealing disc. Notably, the simulation results revealed that altering the diameter of the sealing disc in particular offers a facile means to significantly affect the forces on the disc that prevent the 'open state' (supplementary figure S1 (available online at

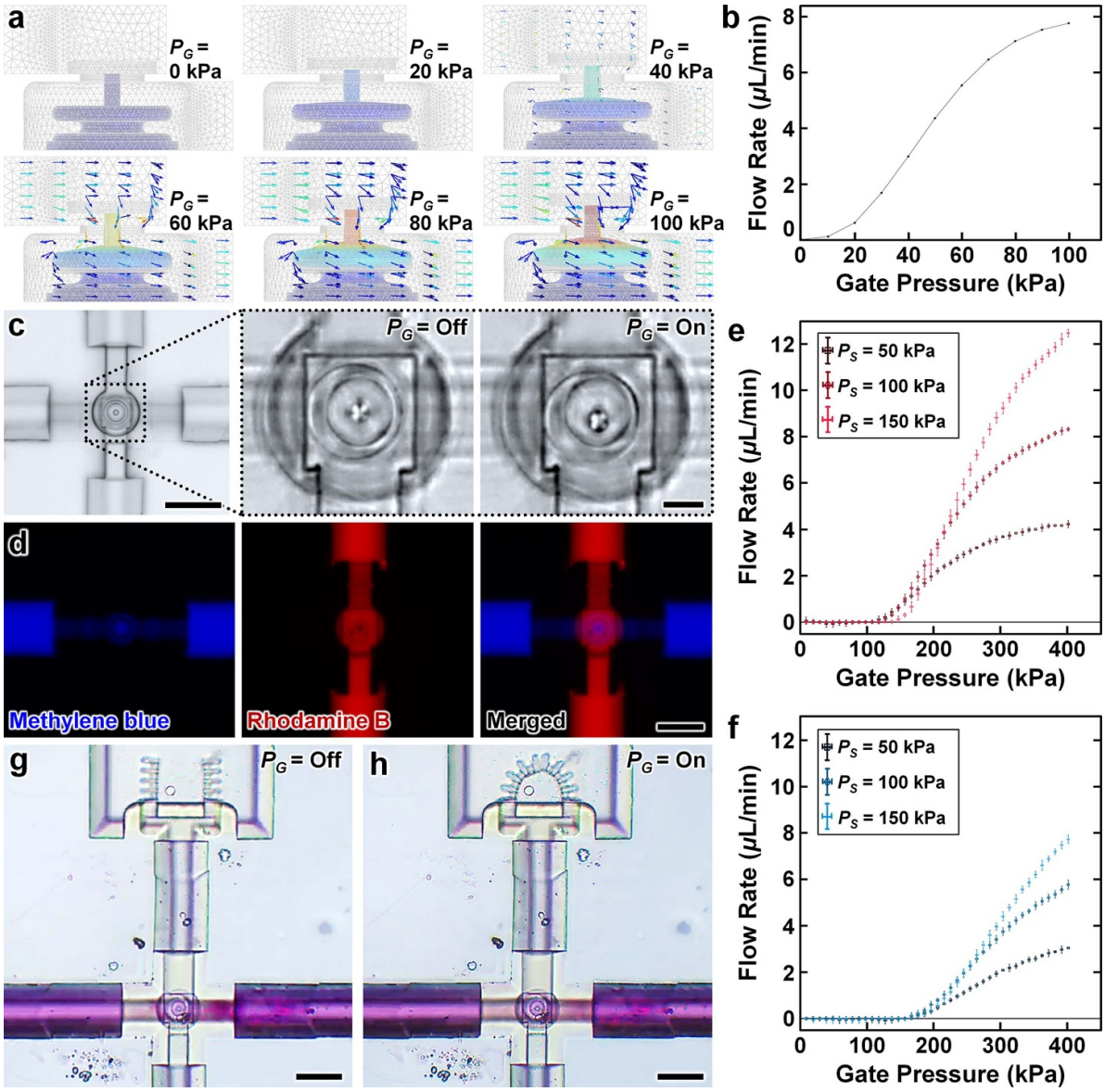

Figure 4. 'Normally closed' microfluidic transistor operation results. (a) Finite element analysis (FEA) fluid-structure interaction (FSI) simulation results for varying P_G ($P_S = 10$ kPa). (b) Simulation results for Q_{SD} *versus* P_G ($P_S = 10$ kPa). (c) Brightfield micrographs of the microfluidic transistor with expanded views corresponding to the: (*left*) 'closed state', and (*right*) 'open state' (see Movie 4). Scale bar = 50 μm; Expanded view scale bar = 10 μm. (d) Fluorescence micrographs corresponding to distinct dyed fluids inputted into the: (*left*) gate microchannel, and (*middle*) source-to-drain microchannel. (*Right*) Merged micrograph. Scale bar = 50 μm. (e), (f) Quantified experimental results for Q_{SD} *versus* P_G at varying P_S for the: (e) D_1 microfluidic transistor (disc diameter = 25 μm), and (f) D_1 microfluidic transistor (disc diameter = 26 μm). Error bars denote S.D.; *See also* supplementary figure S2. (g), (h) An integrated microfluidic system consisting of one microfluidic transistor and one soft microgripper (positioned downstream of the drain) corresponding to the microfluidic transistor: (g) 'closed state', and (h) 'open state' (see Movie 5). Scale bars = 50 μm.

stacks.iop.org/JMM/31/044001/mmedia)), and in turn, govern the gate activation pressure of the microfluidic transistor. Specifically, for a disc located at a distance of 0.1 μm above the orifice, increasing the disc diameter from 25 to 26 μm corresponded to a 19% increase in the resultant (shear and normal) downward forces acting on the sealing disc. To experimentally explore the efficacy of tuning this geometric factor to alter the gate activation pressure required for transitioning from the 'closed state' to the 'open state', we *is*DLW-printed and characterized two distinct microfluidic transistors that differed only in terms of the diameter of the free-floating sealing disc: (i) $D_1 = 25$ μm, and (ii) $D_2 = 26$ μm. To quantify the fluidic performance of each microfluidic transistor, we measured the magnitude of Q_{SD} corresponding to distinct, constant P_S inputs and varying P_G inputs (figures 4(e) and (f)).

Experimental results for the D_1 microfluidic transistor revealed three fundamental operational modes based on the magnitude of the P_G input (figure 4(e)). For lower P_G magnitudes (e.g. $P_G < 100$ kPa), the sealing disc effectively obstructed Q_{SD} for all P_S inputs examined. The second mode involved the gate activation and the corresponding onset of

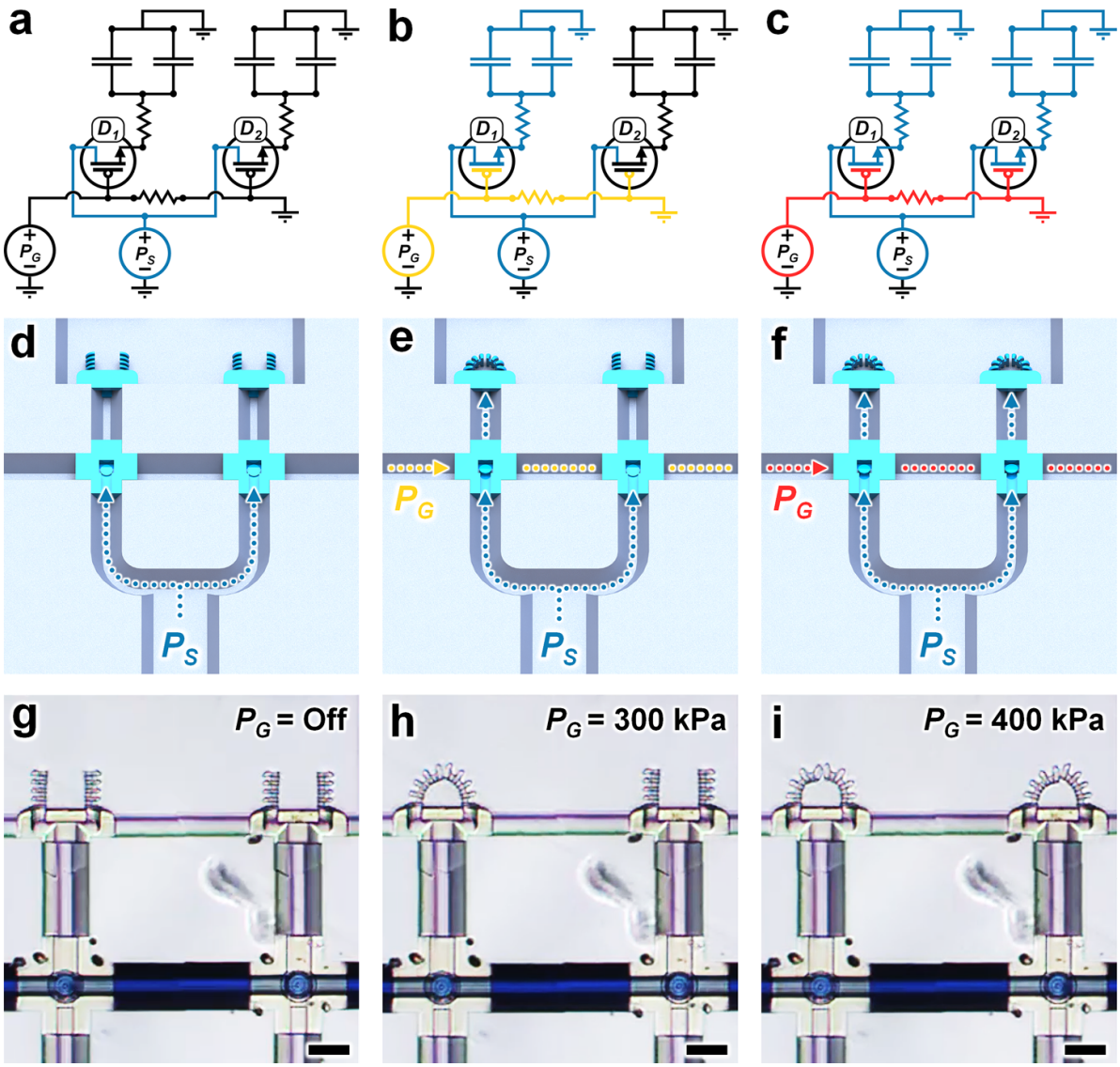

Figure 5. An integrated microfluidic system consisting of the D_1 and D_2 'normally closed' microfluidic transistors with identical soft microgrippers positioned downstream of each drain. (a)–(c) Analogous circuit diagrams and (d)–(f) conceptual illustrations corresponding to the three fundamental operational modes based on a constant P_S input and a single varying P_G input: (a), (d) P_G = Off; (b), (e) P_G = Intermediate (i.e. capable of activating the gate of the D_1 microfluidic transistor, but not that of the D_2 microfluidic transistor); and (c), (f) P_G = High (i.e. capable of activating the gates of both microfluidic transistors). (g)–(i) Brightfield micrographs of experimental results for the microfluidic system under a constant P_S of 100 kPa and distinct P_G magnitudes: (g) P_G = 0 kPa; (h) P_G = 300 kPa; and (i) P_G = 400 kPa (see Movie 6). Scale bars = 50 μm.

Q_{SD}, which occurred for P_G magnitudes in the range of approximately 100–150 kPa for the P_S inputs tested. Consistent with the simulation results (figure 4(b)), we observed a third mode at higher P_G magnitudes as the slope relating Q_{SD} to P_G began decreasing with increasing P_G (figure 4(e)). In particular, for a P_S input of 50 kPa, Q_{SD} appeared to approach a maximum value, after which it is expected that the magnitude of Q_{SD} would instead begin decreasing with increasing P_G. Overall, the results for the D_2 microfluidic transistor were consistent with these trends; however, we found that the increase in the sealing disc diameter resulted in a slight shift in the data toward higher P_G magnitudes (figure 4(f)). For example, the gate activation region instead occurred in the range of approximately 150–175 kPa for the P_S inputs investigated. In addition, the Q_{SD}-P_G relationships for the D_2 microfluidic transistor exhibited reduced slopes (and smaller Q_{SD} magnitudes) compared to their D_1 counterparts (figures 4(e) and (f)). In combination, these results suggest an important role for the sealing disc diameter in regulating the gate activation region. One caveat, however, is that the P_G input should be tailored to particular target conditions rather than increasing the P_G input arbitrarily, as doing so could yield the opposite of the desired effect at higher P_G magnitudes—i.e. unintentionally reestablishing a 'closed state'.

3.3. isDLW-printed integrated 3D microfluidic transistors and soft microgrippers

To initially explore the integration of the 'normally closed' microfluidic transistors with the soft microgrippers, we designed a microfluidic system in which a soft microgripper was printed downstream of the drain of a single microfluidic transistor (figures 4(g) and (h)). First, we applied a constant P_S without any P_G input. In this case, the microfluidic transistor effectively maintained its 'closed state', blocking Q_{SD}, and in turn, precluding unintended microgripper deformation (figure 4(g)). By applying the P_G input, however, the microfluidic transistor transitioned to its 'open state', permitting fluid flow through the component and into the soft microgrippers to yield successful actuation (figure 4(h); Movie 5).

We designed the IFC comprising the two distinct 'normally closed' microfluidic transistors (i.e. corresponding to the D_1 and D_2 discs) and the two sets of soft microgrippers to yield hard-coded operations based on the magnitude of the P_G input (while an applied P_S remains constant at a set magnitude) (figures 5(a)–(f)). Specifically, under a constant P_S input, the functionality of the microfluidic system entails three fundamental P_G-mediated operational modes. In the absence of a P_G input, the P_S causes both microfluidic transistors to enter their 'closed states' and prevent microgripper actuation (figures 5(a) and (d)). A second mode involves the application of an intermediate P_G magnitude that is high enough to yield gate activation for the D_1 microfluidic transistor, but not so for the D_2 microfluidic transistor. As a result, only the D_1 microfluidic transistor is able to transition to the 'open state', and thus, only the first set of microgrippers actuate (figures 5(b) and (e)). Lastly, under a high P_G input, the gates of both the D_1 and D_2 microfluidic transistors are activated (i.e. inducing the 'open state'), resulting in both sets of soft microgrippers actuating (figures 5(c) and (f)).

To experimentally investigate these capabilities, the P_S input was set at a constant magnitude of 100 kPa, while the P_G input was varied between three target magnitudes corresponding to the three operational states: (i) $P_G = 0$ kPa, both microfluidic transistors remained in the 'closed state'—none of the soft microgrippers actuated (figure 5(g)); (ii) $P_G = 300$ kPa, the D_1 microfluidic transistor exhibited gate activation and 'open state' behavior—the corresponding (i.e. downstream) soft microgripper actuated (figure 5(h)); and (iii) $P_G = 400$ kPa, both microfluidic transistors exhibited gate activation and 'open state' behavior—both soft microgrippers actuated (figure 5(i)). During microfluidic testing, we observed that the actuation of the microgrippers was not instantaneous, instead requiring more than one second to deform fully as designed (Movie 6). One potential basis for this trend is that, akin to the time associated with charging an electronic capacitor, so too does each actuator—operating as a fluidic capacitor—necessitate an inflation time to physically expand to store fluid volume. In cases that demand more rapid microgripper actuation capabilities, it is expected that a higher P_S input would reduce such time delays. Nonetheless, these results demonstrate the ability to hard code P_G-mediated operational functionalities into IFC-microrobotic systems.

4. Conclusion

Emerging additive manufacturing strategies hold great promise for advancing the capabilities of IFCs to enhance on-chip autonomy for broad scientific fields. In this work, we leveraged our group's *is*DLW approach [40, 41] to not only introduce 'normally closed' microfluidic transistors for which the gate activation dynamics can be tuned via geometric means, but also demonstrate the incorporation of distinct microfluidic transistors and soft microrobotic end effectors into an integrated hard-coded microfluidic system capable of executing multiple operational states in response to a single varying P_G input. To our knowledge, this work represents the first demonstration of 3D printed normally closed microfluidic transistors as well as the smallest normally closed microfluidic transistors (fabricated by any means) reported in the literature [57–61]. Both theoretical and experimental results revealed that the microfluidic transistor enabled active control of fluid flow through the source-to-drain microchannel through interactions between its two key dynamic components: (i) a bellow microstructure, and (ii) a free-floating sealing disc. Here, the microfluidic transistor comprised a single, relatively rigid photomaterial (i.e. IP-L 780); however, multi-material DLW methodologies [62, 63] could be employed to tailor material properties to functionality (e.g. printing the bellow microstructure with a more flexible material). One caveat to the microfluidic transistor performance was that the top surface of the bellow microstructure appeared to approach the underside of the orifice at high P_G magnitudes, thereby increasing the hydrodynamic resistance through the component, contrary to its intended functionality. To prevent such undesired occurrences, future efforts should investigate the concept of integrating structural members (e.g. microposts) onto the top surface of the bellow microstructure to physically maintain a set surface-to-orifice distance in all cases of high P_G magnitudes.

It is important to note that the presented *is*DLW-based approach for integrating soft robotic components with microfluidic circuit elements could be adapted for larger scale 3D printing methods, such as vat photopolymerization and material jetting technologies. Furthermore, alternative materials allowing for distinct actuation functionalities, such as thermoresponsive [64] rather than microfluidic routines, could be readily incorporated into the presented approach. Unfortunately, the size limitations of DLW could hinder efforts to merge macroscale actuation strategies [65] with the technique in this work. Although the presented fabrication process is based on printing inside of microchannels, the underlying concepts could be adapted to print IFCs integrated with externally printed mechano-fluidic soft robotic components akin to those demonstrated recently [48]. In contrast to standard methods of IFC manufacturing, which rely on microfabrication facilities and user skill-based repeatability, access to the DLW 3D printer in this work represents the only critical barrier in replicating the methods in this work. As the analogues, *p-channel* and *n-channel* transistors, offer distinct benefits in varying electronics scenarios, we anticipate that the ability for researchers to readily harness both 'normally open' [41] and 'normally closed'

microfluidic transistors in 3D IFCs could have important implications for chemical, biomedical, and soft robotics applications.

Data availability statement

All data that support the findings of this study are included within the article (and any supplementary files).

Acknowledgments

We greatly appreciate the contributions of Ryan Utz, Andrew Lamont, Michael Restaino, Ruben Acevedo, Ziteng Wen, and the members of the Bioinspired Advanced Manufacturing (BAM) Laboratory. We also greatly appreciate the help and support of technical staff of the Terrapin Works 3D printing hub at the University of Maryland, College Park. This work was supported in part by NSF Award Numbers 1943356 and 1761395 as well as the US Army Research Laboratory (ARL) Award Number W911NF2020222.

ORCID iDs

Abdullah T Alsharhan https://orcid.org/0000-0002-3037-6127
Olivia M Young https://orcid.org/0000-0001-9883-8538
Xin Xu https://orcid.org/0000-0002-0164-0785
Ryan D Sochol https://orcid.org/0000-0002-9633-8932

References

[1] Sackmann E K, Fulton A L and Beebe D J 2014 *Nature* **507** 181–9
[2] Elvira K S, i Solvas X C, Wootton R C R and deMello A J 2013 *Nat. Chem.* **5** 905–15
[3] Hol F J H and Dekker C 2014 *Science* **346** 1251821
[4] Berlanda S F, Breitfeld M, Dietsche C L and Dittrich P S 2021 Recent Advances in Microfluidic Technology for Bioanalysis and Diagnostics *Anal. Chem.* **93** 311–31
[5] van Lintel H T G, van De Pol F C M and Bouwstra S 1988 *Sensors Actuators* **15** 153–67
[6] Harrison D J, Manz A, Fan Z, Luedi H and Widmer H M 1992 *Anal. Chem.* **64** 1926–32
[7] Harrison D J, Fluri K, Seiler K, Fan Z, Effenhauser C S and Manz A 1993 *Science* **261** 895–7
[8] Whitesides G M 2006 *Nature* **442** 368–73
[9] Aumiller G D, Chandross E A, Tomlinson W J and Weber H P 1974 *J. Appl. Phys.* **45** 4557–62
[10] Duffy D C, McDonald J C, Schueller O J A and Whitesides G M 1998 *Anal. Chem.* **70** 4974–84
[11] Unger M A, Chou H P, Thorsen T, Scherer A and Quake S R 2000 *Science* **288** 113–16
[12] Thorsen T, Maerkl S J and Quake S R 2002 *Science* **298** 580–4
[13] Lee C *et al* 2005 *Science* **310** 1793–6
[14] Balagaddé F K, You L, Hansen C L, Arnold F H and Quake S R 2005 *Science* **309** 137–40
[15] Mosadegh B, Bersano-Begey T, Park J Y, Burns M A and Takayama S 2011 *Lab Chip* **17** 2813–18
[16] Leslie D C, Easley C, Seker E, Karlinsey J M, Utz M, Begley M R and Landers J P 2009 *Nat. Phys.* **5** 231–5
[17] Mosadegh B, Kuo C H, Torisawa Y S, Bersano-Begey T, Tavana H and Takayama S 2010 *Nat. Phys.* **6** 433–7
[18] Weaver J A, Melin J, Stark D, Quake S R and Horowitz M A 2010 *Nat. Phys.* **6** 218–23
[19] Li Z and Kim S 2019 *Sci. Adv.* **5** eaat3080
[20] Rothemund P, Ainla A, Belding L, Preston D J, Kurihara S, Suo Z and Whitesides G M 2018 *Sci. Robot.* **3** eaar7986
[21] Napp N, Araki B, Tolley M T, Nagpal R and Wood R J 2014 Simple passive valves for addressable pneumatic actuation *2014 IEEE Int. Conf. on Robotics and Automation (ICRA)* pp 1440–5
[22] Wehner M, Truby R L, Fitzgerald D J, Mosadegh B, Whitesides G M, Lewis J A and Wood R J 2016 *Nature* **536** 451–5
[23] Iwai K, Shih K C, Lin X, Brubaker T A, Sochol R D and Lin L 2014 *Lab Chip* **14** 3790–9
[24] Bhattacharjee N, Urrios A, Kang S and Folch A 2016 *Lab Chip* **16** 1720–42
[25] Sochol R D, Casavant B P, Dueck M E, Lee L P and Lin L 2011 *J. Micromech. Microeng.* **21** 054019
[26] Au A K, Huynh W, Horowitz L F and Folch A 2016 *Angew. Chem., Int. Ed.* **55** 3862–81
[27] Sochol R D, Lu A, Lei J, Iwai K, Lee L P and Lin L 2014 *Lab Chip* **14** 1585–94
[28] Nielsen A V, Beauchamp M J, Nordin G P and Woolley A T 2020 *Annu. Rev. Chem.* **13** 45–65
[29] Su R, Wen J, Su Q, Wiederoder M S, Koester S J, Uzarski J R and McAlpine M C 2020 *Sci. Adv.* **6** eabc9846
[30] Au A K, Bhattacharjee N, Horowitz L F, Chang T C and Folch A 2015 *Lab Chip* **15** 1934–41
[31] Gong H, Woolley A T and Nordin G P 2016 *Lab Chip* **16** 2450–8
[32] Rogers C I, Qaderi K, Woolley A T and Nordin G P 2015 *Biomicrofluidics* **9** 016501
[33] Bhargava K C, Thompson B and Malmstadt N 2014 *Proc. Natl Acad. Sci. USA* **111** 15013–18
[34] Lee Y S, Bhattacharjee N and Folch A 2018 *Lab Chip* **18** 1207–14
[35] Sochol R D *et al* 2016 *Lab Chip* **16** 668–78
[36] Sweet E, Mehta R, Xu Y, Jew R, Lin R and Lin L 2020 *Lab Chip* **20** 3375–85
[37] Childs E H, Latchman A V, Lamont A C, Hubbard J D and Sochol R D 2020 *J. Microelectromech. Syst.* **29** 1094–6
[38] Hahn V, Kiefer P, Frenzel T, Qu J, Blasco E, Barner-Kowollik C and Wegener M 2020 *Adv. Funct. Mater.* **30** 1907795
[39] Lölsberg J, Cinar A, Felder D, Linz G, Djeljadini S and Wessling M 2019 *Small* **15** 1901356
[40] Lamont A C, Alsharhan A T and Sochol R D 2019 *Sci. Rep.* **9** 394
[41] Alsharhan A T, Acevedo R, Warren R and Sochol R D 2019 *Lab Chip* **19** 2799–2810
[42] Chen S, Cao Y, Sarparast M, Yuan H, Dong L, Tan X and Cao C 2020 *Adv. Mater. Technol.* **5** 1900837
[43] Preston D J *et al* 2019 *Sci. Robot.* **4** eaaw5496
[44] Preston D J, Rothemund P, Jiang H J, Nemitz M P, Rawson J, Suo Z and Whitesides G M 2019 *Proc. Natl Acad. Sci.* **116** 7750–9
[45] Soreni-Harari M, St Pierre R, McCue C, Moreno K and Bergbreiter S 2020 *Soft Robot.* **7** 59–67
[46] Cabanach P, Pena-Francesch A, Sheehan D, Bozuyuk U, Yasa O, Borros S and Sitti M 2020 *Adv. Mater.* **32** 2003013
[47] Velez C, Patel D K, Kim S, Babaei M, Knick C R, Smith G L and Bergbreiter S 2020 *J. Microelectromech. Syst.* **29** 867–73

[48] Barbot A, Power M, Seichepine F and Yang G Z 2020 *Sci. Adv.* **6** eaba5660
[49] Montinaro E, Grisi M, Letizia M C, Petho L, Gijis M A M, Guidetti R, Brugger J and Boero G 2018 *PLoS One* **13** e0192780
[50] Alsharhan A T, Stair A J, Acevedo R, Razaulla T, Warren R and Sochol R D 2020 *J. Microelectromech. Syst.* **29** 906–11
[51] Marino A, Tricinci O, Battaglini M, Filippeschi C, Mattoli V, Sinibaldi E and Ciofani G 2018 *Small* **14** 1702959
[52] Lölsberg J, Linkhorst J, Cinar A, Jans A, Kuehne A J C and Wessling M 2018 *Lab Chip* **18** 1341–8
[53] Shepherd R F, Ilievski F, Choi W, Morin S A, Stokes A A, Mazzeo A D, Chen X, Wang M and Whitesides G M 2011 *Proc. Natl Acad. Sci.* **108** 20400–3
[54] Mosadegh B *et al* 2014 *Adv. Funct. Mater.* **24** 2163–70
[55] Lemma E D, Rizzi F, Dattoma T, Spagnolo B, Sileo L, Qualtieri A, De Vittorio M and Pisanello F 2017 *IEEE Trans. Nanotechnol.* **16** 23–31
[56] Alsharhan A T, Stair A J, Utz R R, Lamont A C, Restaino M A, Acevedo R and Sochol R D 2020 *IEEE 33rd Int. Conf. on Micro Electro Mechanical Systems (MEMS)* (https://doi.org/10.1109/MEMS46641.2020.9056155)
[57] Mosadegh B, Tavana H, Lesher-Perez S C and Takayama S 2011 *Lab Chip* **11** 738–42
[58] Kim J, Kang M, Jensen E C and Mathies R A 2012 *Anal. Chem.* **84** 2067–71
[59] Rahmanian O D and DeVoe D L 2015 *Microfluidics Nanofluidics* **18** 1045–53
[60] Li K, Morton K, Shiu M, Turcotte K, Lukic L, Veilleux G, Poncelet L and Veres T 2020 *IEEE 33rd Int. Conf. on Micro Electro Mechanical Systems (MEMS)* (https://doi.org/10.1109/MEMS46641.2020.9056136)
[61] Kim J, Stockton A M, Jensen E C and Mathies R A 2016 *Lab Chip* **16** 812–19
[62] Lamont A C, Restaino M A, Kim M J and Sochol R D 2019 *Lab Chip* **19** 2340–5
[63] Mayer F, Richter S, Westhauser J, Blasco E, Barner-Kowollik C and Wegener M 2019 *Sci. Adv.* **5** eaau9160
[64] Nishiguchi A, Zhang H, Schweizerhof S, Schulte M F, Mourran A and Möller M 2020 *ACS Appl. Mater. Interfaces* **12** 12176–85
[65] Soon R H, Yu L and Lim C T 2020 *Adv. Mater. Technol.* **5** 2000150